Received XX Month XXXX; revised X Month XXXX; accepted XX Month XXXX. Date of publication XX Month XXXX; date of current version XX Month XXXX.

Digital Object Identifier 10.1109/OAJPE.2020.2976889

Design of Optimal Gain Mask for Phased Array-Fed Offset Reflectors

MINSANG YOON[1], CHANGHYEON IM[1], CHANGSUNG KIM[2], WONGU SEO[2], SEULGI PARK[2], AND HOSUNG CHOO[1], SENIOR MEMBER, IEEE

[1]Department of Electronic and Electrical Engineering, Hongik University, Seoul 04066, South Korea

[2]Hanwha Systems, Yougin 1712, South Korea

CORRESPONDING AUTHOR: C. Im (e-mail: b615171@mail.hongik.ac.kr)

This work was supported by Korea Research Institute for Defense Technology Planning and Advancement (KRIT) grant funded by Defense Acquisition Program Administration (DAPA), 21-307-A00-013, Korea BFT Communication Satellite Large Antenna Technology.

ABSTRACT In this paper, we propose a method to derive an optimal gain mask to enhance the aperture efficiency of phased array-fed reflectors (PAFRs). The optimal gain mask is obtained to uniformly illuminate the offset reflector's surface. The optimal gain mask is derived based on the square of the distances from the feed antenna to each point on the offset reflector surface. To generate a feed pattern similar to the optimal gain mask, a 4 × 8 array antenna is used as the feed antenna. Using this array antenna, beam synthesis is applied through the superposition of array patterns sampled at 1° intervals in both θ and ϕ. In addition, to achieve sidelobe suppression, quadratic taper function is applied to the derived optimal gain mask. We then illuminate the reflector using three feed patterns: a synthesized beam based on the proposed mask, a synthesized beam following a cosecant-squared mask, and a single horn antenna pattern. In this case, the same quadratic tapering order of $N = 0.5$ is applied to both the proposed gain mask and the cosecant-squared mask. The proposed method shows a bore-sight gain of 48.2 dBi and a sidelobe level (SLL) of −39.0 dB, representing improvements compared with the results obtained using the cosecant-squared-based pattern (47.5 dBi and −35.8 dB) and the horn antenna pattern (47.8 dBi and −34.0 dB). These results demonstrate that the proposed gain mask and beam synthesis method are effective in achieving high aperture efficiency and sidelobe suppression performance.

INDEX TERMS PAFR, offset reflector antenna, beam synthesis, aperture efficiency, phased array antenna.

I. INTRODUCTION

Modern satellites are utilized in various RF applications, including mobile communications [1], military tactical communications [2], and signal intelligence (SIGINT) [3]. In these systems, high-gain antennas are required to compensate for the path loss caused by the long distance between satellites and Earth stations [4], [5]. Accordingly, reflector antennas are generally used because they have high-gain characteristics through large-diameter reflectors, such as Cassegrain reflectors, front-feed reflectors, and offset reflectors [6], [7], [8]. In particular, offset reflector antennas are widely employed because they can effectively minimize structural blockage and simplify mechanical structures [9]. To transport these large-diameter reflector antennas to operational altitudes, they should be mounted on a launch vehicle, which has strict constraints on payload volume and weight [10], [11]. Therefore, it is necessary to enhance the aperture efficiency of a limited-size reflector to achieve high-gain performance. Moreover, effective sidelobe suppression is required to mitigate undesired interference and improve the signal-to-interference ratio (SIR) [12]. To address these issues, several studies have focused on designing matched feeds with an optimized beamwidth to minimize spillover [13], [14]. These studies have enhanced aperture efficiency through beamwidth optimization but there are limits to improving the efficiency of an offset reflector using a single antenna due to the asymmetric geometry of the reflector [15]. Subsequently, research has reported the use of a phased array-fed reflector (PAFR) system to achieve high aperture efficiency of the offset reflector, enabling more uniform illumination over their asymmetric geometry [16]. In PAFR systems, conjugate-field matching (CFM) provides an optimal solution for maximizing the gain [17], [18]. However, it requires full-wave simulations for each excitation port, which significantly increases computational complexity, particularly for large-scale reflector systems [19]. To avoid computational complexity, mask-based beam synthesis approaches for feeders have been studied [20]. This study demonstrated that synthesizing a cosecant-squared beam pattern in the feed's elevation direction can achieve an aperture efficiency of up to 60% of the PAFR. In addition, studies have been conducted to analyze the main lobe gain and sidelobe suppression performance of reflectors based on the current distribution over the surface [21], [22], [23] However, these studies have not proposed an optimal gain mask that maximizes aperture efficiency by precisely accounting for the asymmetric geometry of offset reflectors, nor have they used a beam synthesizing method to obtain such a pattern. Furthermore, limited research has been done in applying taper functions to the derived optimal gain mask and quantitatively evaluating the trade-off between the main lobe gain and the sidelobe level (SLL) as a function of edge taper strength.

In this paper, we propose a method to derive the optimal gain mask necessary to maximize the aperture efficiency of PAFR. The optimal gain mask is obtained to provide uniform illumination on the offset reflector surface; thus, it is determined based on the square of the distances from the feed antenna to each point on the offset reflector surface. To achieve a feed pattern resembling the optimal gain mask, a 4 × 8-phased array feed (PAF) is utilized. Beam synthesis is performed by the superposition of array patterns steered in each direction and weighted according to the corresponding mask value. The mask is sampled at 1° increments in both θ and ϕ. Since the sampling density decreases as θ increases, a $\sin(\theta)$ is applied as a weighting factor to compensate for the non-uniform sampling density. In addition, a quadratic taper function is applied to the gain mask to suppress the sidelobes of the reflector's radiation pattern. We then illuminate the reflector using three feed patterns: a synthesized beam following the proposed mask, a synthesized beam following a cosecant-squared mask, and a single horn antenna pattern. The proposed mask achieves enhanced aperture efficiency and an SLL compared with the results obtained using the cosecant-squared-based pattern and the horn antenna pattern. In addition, to analyze the performance with edge tapering, we conducted simulations by applying a quadratic taper function to the gain mask. The proposed feed pattern also achieves higher reflector aperture efficiency and lower SLL than the cosecant-squared-based pattern and the single horn antenna pattern.

The paper is organized as follows. In Section II, we describe the geometry of the PAFR and the derivation process of the gain mask of the feed antenna. In Section III, the beam synthesis method is used to approximate the gain mask, and a taper function is applied to suppress the SLL. In Section IV, full-wave simulations validate the proposed method by comparing gain and sidelobe performance with reference methods.

II. FEEDER OPTIMAL GAIN MASK DERIVATION

Figure 1 illustrates the geometry of an offset reflector antenna and a method for enhancing the effective illumination area of the reflector. The surface of the offset reflector is designed by applying the parabolic equation with a focal length of F [24], which has a diameter of D and an offset angle of ψ, as shown in Figure 1(a). In this configuration, when the feed antenna is located at the focal point of the parabolic surface, the field reflected by the surface has an equal-phase distribution across the aperture, resulting in constructive interference along the bore-sight [25]. In an offset reflector antenna, the reflector exhibits edge-to-edge angles θ_{Ver} and θ_{Hor} in the vertical and horizontal planes with respect to the focal point. Accordingly, the feed pattern must be designed considering θ_{Ver} and θ_{Hor} to enhance the reflector's aperture efficiency. Figure 1(b) illustrates the effective reflection area of the offset reflector according to feed antenna type. The offset reflector antenna has different distances from the focal point to the low- and high-elevation edges, denoted by d_l and d_u, where d_l is smaller than d_u. The larger path length d_u results in a greater reduction in field magnitude relative to that for d_l [26]. In this geometry, a single-feed antenna is limited in compensating for the magnitude difference, which reduces the effective reflection area and consequently degrades aperture efficiency. To overcome this limitation, PAF can be employed as the feed, which generates a synthesized pattern that accounts for asymmetric geometry. By shaping the feed pattern to provide a higher gain toward the longer paths and a lower gain toward the shorter paths, a larger effective reflection area can be achieved compared to a single-feed antenna.

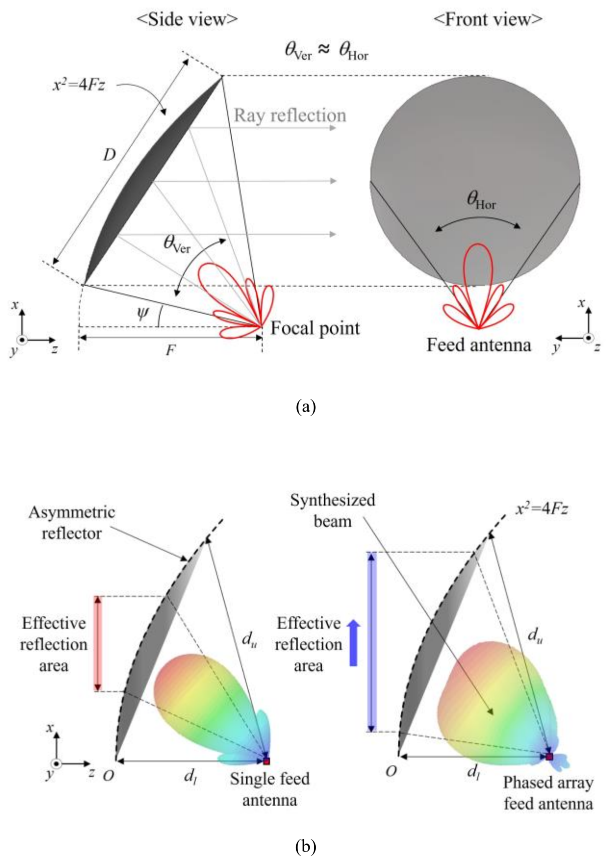

FIGURE 1. The geometry of the offset reflector antenna and the effective reflection area. (a) Geometry of the circular offset reflector antenna. (b) Phased array feed (PAF) to improve the effective reflection area.

Figure 2 shows the method for deriving the optimal gain mask that maximizes the aperture efficiency of the offset reflector. The proposed method ensures uniform surface current distribution by accounting for the distance between the feed antenna and each point of the reflector surface. To calculate these distances, a local coordinate system is defined such that the feed bore-sight is equal to the local z-axis ($\hat{z}$), as shown in Figure 2(a). Here, the x-axis of the local coordinate system ($\hat{x}$) is aligned parallel to the y-axis of the global coordinate system. Here, v_{local} denotes the local unit vector pointing in the (θ_l, ϕ_l) direction with respect to the feed. The distance from the feed to each point on the reflector surface is calculated using the following equations (1)-(4) [27]:

$$M_{\text{Rot}} = \begin{bmatrix} 0 & \cos(\alpha) & \sin(\alpha) \\ 1 & 0 & 0 \\ 0 & \sin(\alpha) & -\cos(\alpha) \end{bmatrix} \tag{1}$$

$$v_{\text{local}} = \begin{bmatrix} \sin(\theta_l)\cos(\phi_l) \\ \sin(\theta_l)\sin(\phi_l) \\ \cos(\theta_l) \end{bmatrix} \tag{2}$$

$$P_{\text{global}}(x_p, y_p, z_p) = \overrightarrow{OP_F} + r(M_{\text{Rot}}^T \cdot v_{\text{local}}) \tag{3}$$

$$\begin{bmatrix} x_p \\ y_p \\ z_p \end{bmatrix} = \begin{bmatrix} r\sin(\theta_l)\sin(\phi_l) \\ r(\sin(\theta_l)\cos(\phi_l)\cos(\alpha) + \cos(\phi_l)\cos(\alpha)) \\ F + r(\sin(\theta_l)\cos(\phi_l)\sin(\alpha) - \cos(\phi_l)\cos(\alpha)) \end{bmatrix} \tag{4}$$

$$R(\theta_l, \phi_l) = \{r \mid x_p^2 + y_p^2 = 4Fz_p,\ r > 0\} \tag{5}$$

where M_{Rot} represents the rotation matrix to transform v_{local} into the global coordinate vector. The α denotes the elevation angle of the feed bore-sight, defined as the tilt angle of the local z-axis. Here, the bore-sight direction angle ($\alpha = \psi + \theta_{\text{Ver}}/2$) is the bisector of the $\overrightarrow{P_F P_l}$ and $\overrightarrow{P_F P_u}$. The unit vector v_{local} is defined in the local coordinate system, directed from the feed to the reflector surface, where θ_l and ϕ_l denote its θ and ϕ direction in the local spherical coordinates, respectively. The $P_{\text{global}}(x_p, y_p, z_p)$, representing the global position vector on the parabola surface in the (θ_l, ϕ_l) direction, is then obtained by transforming v_{local} into the global coordinate system, while $\overrightarrow{OP_F}$ indicates the feed position in the global coordinates, and r represents the distance along the unit vector $M_{\text{Rot}}^{\text{T}} \cdot v_{\text{local}}$ from the feed toward the reflector surface. Parameter r can be determined by substituting $P_{\text{global}}(x_p, y_p, z_p)$ into the parabolic equation in the global coordinates, as shown in equation (5). The positive solution of r corresponds to the feed-to-reflector distance in the (θ_l, ϕ_l) direction, which is defined as $R(\theta_l, \phi_l)$. In addition, to determine the required beamwidth of the feed, θ_{Ver} should be calculated, and for this, the coordinate values of $P_l(x_l, y_l, z_l)$ and $P_u(x_u, y_u, z_u)$ need to be derived. The lower edge coordinate P_l can be determined by using equations (6), and (7).

$$P_l(x_l, y_l, z_l) = \left(\overline{P_F P_l}\sin(\psi),\ 0,\ F - \overline{P_F P_l}\cos(\psi)\right) \tag{6}$$

$$\overline{P_F P_l} = \frac{2F(1-\cos(\psi))}{\sin^2(\psi)} \tag{7}$$

The upper edge coordinate $P_u(x_u, y_u, z_u)$ can be determined by using equations (8), and (9):

$$P_u(x_u, y_u, z_u) = \left(x_u,\ 0,\ \frac{x_u^2}{4F}\right) \tag{8}$$

$$x_u = \left\{x \mid (x - x_l)^2 + \left(\frac{x^2}{4F} - z_l\right)^2 = D^2,\ x > 0\right\} \tag{9}$$

where z_u can be obtained by substituting (x_u, 0, z_u) in the parabolic equation (4). The coordinate x_u is determined as the positive solution that satisfies $\overline{P_l P_u} = D$ on the parabolic surface. Consequently, the θ_{Ver} is calculated as the angle between the vectors $\overrightarrow{P_F P_l}$ and $\overrightarrow{P_F P_u}$ as the following equation:

$$\theta_{\text{Ver}} = \cos^{-1}\left(\frac{\overrightarrow{P_F P_l} \cdot \overrightarrow{P_F P_u}}{\|\overrightarrow{P_F P_l}\|\|\overrightarrow{P_F P_u}\|}\right) \tag{10}$$

Following this procedure, equations (1)-(10), we can obtain a normalized gain mask $G(\theta_l, \phi_l)$ proportional to $R^2(\theta_l, \phi_l)$, as represented in Figure 2(b). Since the radiated power from the feed attenuates proportionally to the square of the distance, a feed radiation pattern proportional to $R^2(\theta_l, \phi_l)$ can provide uniform illumination across the reflector surface. This mask is derived for the case of offset angle $\psi = 0°$, reflector diameter $D = 10$ m, focal length $F = 6$ m, and edge-to-edge angles ($\theta_{\text{Ver}} = 76°$, $\theta_{\text{Hor}} = 76°$). For computational convenience in beam synthesis, we apply the approximation $\theta_{\text{Ver}} \simeq \theta_{\text{Hor}}$ [28], so the horizontal edge-to-edge angle subtended at the feed can also be considered as 76°. The origin (0, 0) of the uv-plot corresponds to the bore-sight of the feed antenna. With $\overline{P_F P_l} = 6$ m and $\overline{P_F P_u} = 9.6$ m, the required gain toward the upper edge is confirmed to be approximately 4 dB higher than that toward the lower edge.

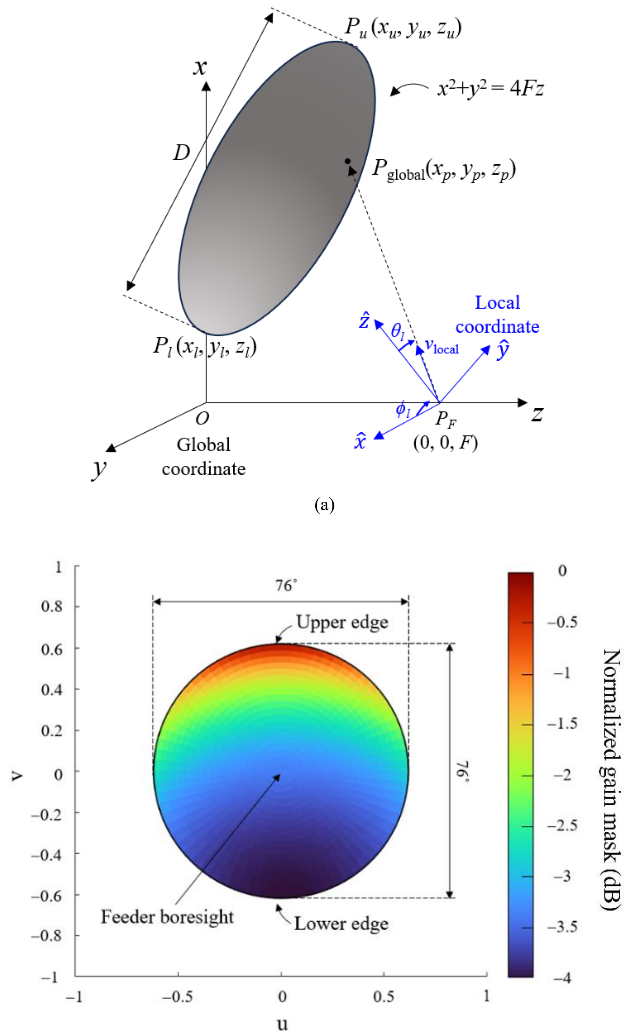

(b)

FIGURE 2. Derivation of an optimal gain mask. (a) Definition of the global and local coordinates of the offset reflector antenna. (b) Derived optimal gain mask.

III. BEAM SYNTHESIS AND EDGE TAPERING

Figure 3 shows the proposed beam synthesis method for obtaining a desired feed pattern by combining array patterns. To generate a synthesized beam pattern based on the derived optimal gain mask, a planar array antenna is required, as shown in Figure 3(a). The broadside direction of the PAF is oriented along the $\hat{\boldsymbol{z}}$ direction of the local coordinate system that was also illustrated in Figure 2(a). This antenna consists of an $M \times N$ array, with element spacings of d_x and d_y along the $\hat{x}$-axis and $\hat{y}$-axis, respectively. Array patterns are then generated for each (θ, ϕ) direction. Here, the array pattern shown in the figure is presented as an example of one of the array patterns generated to synthesize a pattern similar to the gain mask. To generate each array pattern, the complex signal (amplitude and phase) required for each array element is calculated using equations (11)-(13).

$$w_{(\theta',\phi')} = \begin{bmatrix} e^{-jk(x_1u'+y_1v')} & \ddots & \cdots & e^{-jk(x_1u'+y_Nv')} \\ \vdots & & e^{-jk(x_mu'+y_nv')} & \vdots \\ e^{-jk(x_Mu'+y_1v')} & & \cdots \ \ddots & e^{-jk(x_Mu'+y_Nv')} \end{bmatrix} \quad (11)$$

$$u' = \sin(\theta')\cos(\phi'),\ v' = \sin(\theta')\sin(\phi') \quad (12)$$

$$x_m = \left(m - \frac{M+1}{2}\right)d_x,\ y_n = \left(n - \frac{N+1}{2}\right)d_y \quad (13)$$

Where $w_{(\theta',\phi')}$ denotes the steering weight applied to the $M \times N$ planar array elements to steer the array pattern toward (θ', ϕ'), and k is the wavenumber. The array pattern corresponding to this steering weight is calculated as follows:

$$F_{(\theta',\phi')} = \sum_{m=1}^{M}\sum_{n=1}^{N} w_{(\theta',\phi')}(m, n)e^{jk(x_m\sin(\theta)\cos(\phi)+y_n\sin(\theta)\sin(\phi))} \quad (14)$$

where $F_{(\theta',\phi')}$ denotes the array pattern obtained when the corresponding weight $w_{(\theta',\phi')}$ is applied as the input excitation. $w_{(\theta',\phi')}(m, n)$ represents the steering weight of an element located at the m^{th} position along the $\hat{x}$-axis and n^{th} position along the $\hat{y}$-axis. In the spherical coordinate, employing uniform angular steps $(\Delta\theta, \Delta\phi)$ over (θ, ϕ) results in fewer array patterns per unit area at a larger θ. For example, with two elevation angles θ_1 (small) and θ_2 (large), the sampling density along each elevation is proportional to $1/(2\pi\sin\theta_1)$ and $1/(2\pi\sin\theta_2)$, respectively. To synthesize a beam pattern that conforms to the required mask, $\sin(\theta')$ is applied as a weighting factor to compensate for the non-uniform sampling density. Subsequently, using the superposition of array patterns, a beam pattern that resembles the desired mask can be synthesized, as shown in Figure 3(b) [29], [30]. The weight applied to each array element for beam synthesis is calculated using the following equations:

$$w_{syn} = \sum_{\theta'=1°}^{\theta_{Ver}/2}\sum_{\phi'=1°}^{360°} \sin(\theta')\sqrt{G(\theta',\phi')}\, w_{(\theta',\phi')} \quad (15)$$

where w_{syn} denotes the synthesized weight applied to the uniform planar array (UPA) elements. The array patterns are generated for all (θ', ϕ') directions within the edge-to-edge beamwidth at 1° intervals in both θ and ϕ. The weighting factor $\sin(\theta')$ is applied to compensate for non-uniform sampling density. Here, $G(\theta', \phi')$ is the gain mask, while $w_{(\theta',\phi')}$ denotes the steering weight obtained from equation (11). Applying the synthesized weight, the synthesized far-field pattern can then be calculated as follows:

$$F_{syn} = \sum_{m=1}^{M}\sum_{n=1}^{N} w_{syn}(m, n)e^{jk(x_m\sin(\theta)\cos(\phi)+y_n\sin(\theta)\sin(\phi))} \quad (16)$$

F_{syn} denotes the synthesized pattern obtained when the synthesized weight w_{syn} is applied as the excitation, and the $w_{syn}(m, n)$ is the synthesized weight of the (m, n) antenna element obtained from equation (15).

Figure 4 shows the patterns synthesized by applying taper function to the gain mask $G(\theta', \phi')$. A tapered feed pattern is

This article has been accepted for publication in IEEE Open Journal of Antennas and Propagation. This is the author's version which has not been fully edited and content may change prior to final publication. Citation information: DOI 10.1109/OJAP.2026.3696230

required to suppress the edge currents that generate the sidelobes in the PAFR. The taper function is designed such that the gain decreases as the angular distance from the feed center increases, and it is expressed as follows:

$$T(\theta)=\left[1-\left(\frac{\theta}{\theta_{\mathrm{Ver}}/2}\right)^2\right]^N \tag{17}$$

where $T(\theta)$ is a quadratic edge taper function whose magnitude decreases as θ increases from the beam center toward the angular edge. Here, N is the taper order that determines the degree of tapering and θ_{Ver} is the edge-to-edge beamwidth from the feed toward the reflector, as calculated in equation (10). By applying the quadratic taper function to the gain mask $G(\theta', \phi')$, the resulting synthesized PAF weight is expressed as follows:

$$w_T=\sum_{\theta'=1^\circ}^{\theta_{\mathrm{Ver}}/2}\sum_{\phi'=1^\circ}^{360^\circ}\sin(\theta')\sqrt{G(\theta',\phi')\cdot T(\theta')}\cdot w_{(\theta',\phi')} \tag{18}$$

where w_T denotes the weight for the $M{\times}N$ array used to generate the synthesized pattern with tapering. The synthesized pattern obtained using the weight w_T is given as follows:

$$F_{syn.T}=\sum_{m=1}^{M}\sum_{n=1}^{N}w_T(m,n)e^{jk(x_m\sin(\theta)\cos(\phi)+y_n\sin(\theta)\sin(\phi))} \tag{19}$$

$F_{syn.T}$ represents the synthesized pattern with the taper applied to the gain mask. $w_T(m, n)$ is the complex excitation applied to the (m, n)-th element of the PAF. Using the equation (19), we can derive the synthesized pattern for the case where $M = 4$, $N = 8$, and $d_x = d_y = \lambda/2$. By applying taper orders of $N = 0$, 0.5, and 1.0, the corresponding synthesized patterns can be obtained, as shown in Figures 4(a), (b), and (c), respectively. Each antenna element pattern is assumed to be an ideal isotropic pattern. Since θ_{Ver} is 76°, the beam is synthesized up to $\theta = 38°$ along the mask. The radiation patterns in the zx-plane for different taper orders N are shown in Figure 4(d) with the gain mask. For $N = 0$, the normalized gains at the upper and lower edges are −5.5 dB and −9.5 dB, showing that the gain in the upper edge direction is 4 dB higher than that toward the lower edge, which is in good agreement with the mask. When N increases to 0.5, the normalized gains to the edge are reduced to −9.5 dB and −13.3 dB, and for $N = 1.0$, they decrease to −12.2 dB and −15.1 dB, respectively. Therefore, increasing the value of N effectively decreases the gain of the synthesized PAF beam pattern to the reflector's edge. When the three patterns generated for taper orders $N = 0$, 0.5, and 1.0 are used to illuminate the offset reflector ($D = 10$ m, $F = 6$ m, and $\psi = 0°$), the resulting aperture efficiencies are 82.2%, 80.6%, and 78.1%, respectively.

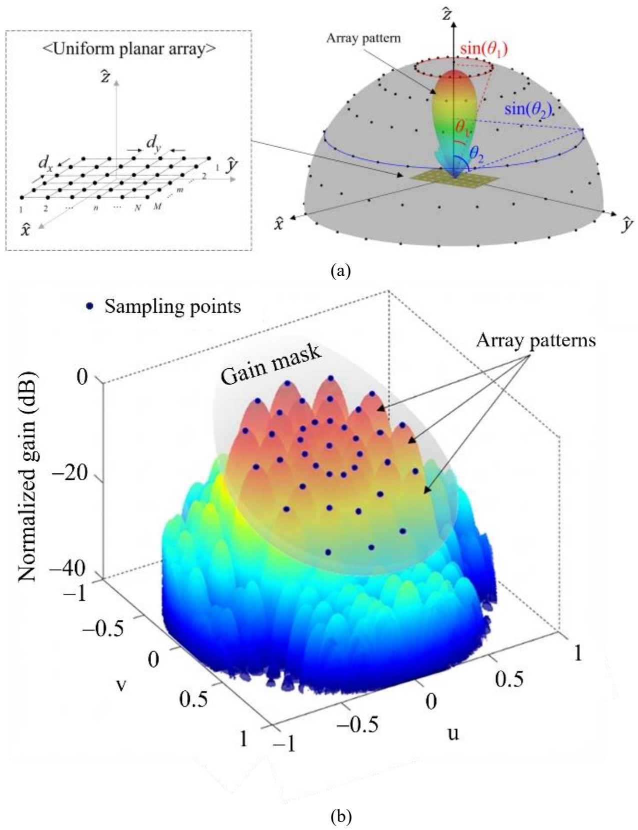

FIGURE 3. Proposed beam synthesis method. (a) Array pattern generation and differential sampling density. (b) Superposition of array patterns with gain mask weighting.

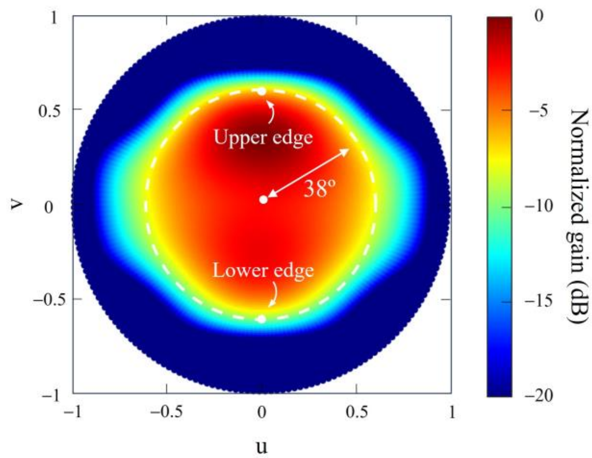

(a)

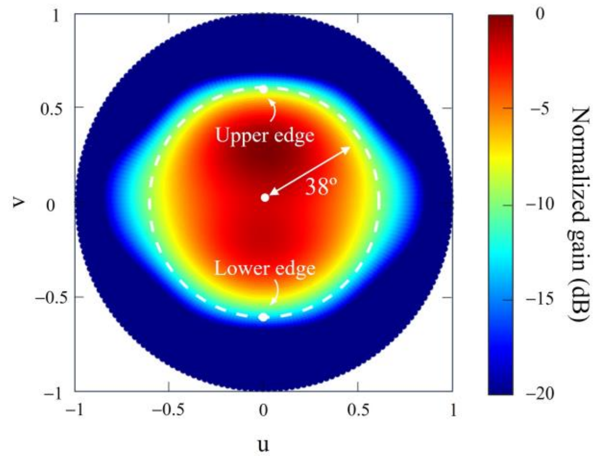

(b)

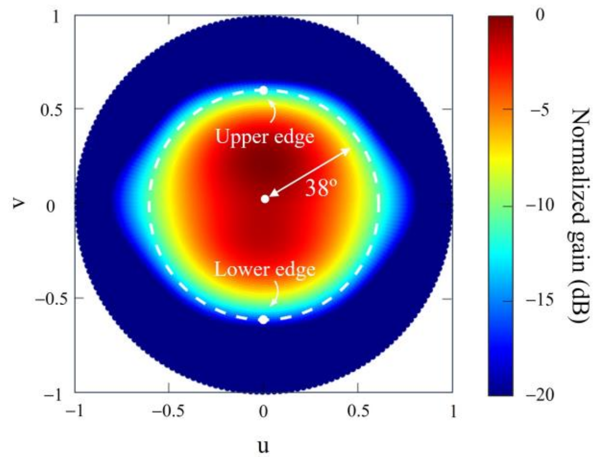

(c)

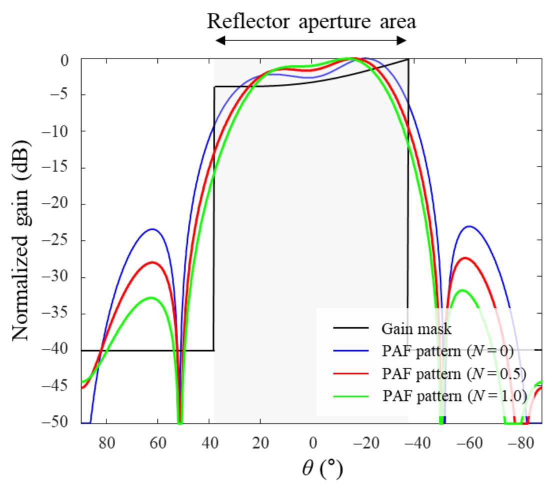

(d)

FIGURE 4. PAF pattern with quadratic taper function. (a) PAF pattern with *N* = 0. (b) PAF pattern with *N* = 0.5. (c) PAF pattern with *N* = 1.0. (d) Synthesized PAF patterns and gain mask in *zx*-plane.

IV. ANALYSIS

Figure 5 shows the simulation setup for the PAFR. Since the optimal gain mask illustrated in Figure 2(b) shows an asymmetric beam pattern in the vertical direction, 8 elements are arranged vertically to provide greater degrees of freedom (DoF) and pattern representation capability compared to the horizontal direction [31]. The feed antenna is designed as a 4 × 8 PAF operating at 3 GHz (S-band), a frequency widely used in satellite communication systems. The patch antenna is implemented on a 1.6 mm Taconic RF-35 substrate ($\varepsilon_r = 3.5$, $tan\delta = 0.0018$), and the array element spacing is set to 0.5λ. Table 1 presents the simulation setup parameters of the offset reflector. The reflector diameter is set to $D = 10$ m, the focal length is set to $F = 6$ m, and the offset angle is set to $\psi = 0°$. The reflector is modeled as an ideal PEC surface, and the feed bore-sight angle ($\theta_{bore\text{-}sight}$) is oriented at 38°, corresponding to half of the edge-to-edge angle of 76°.

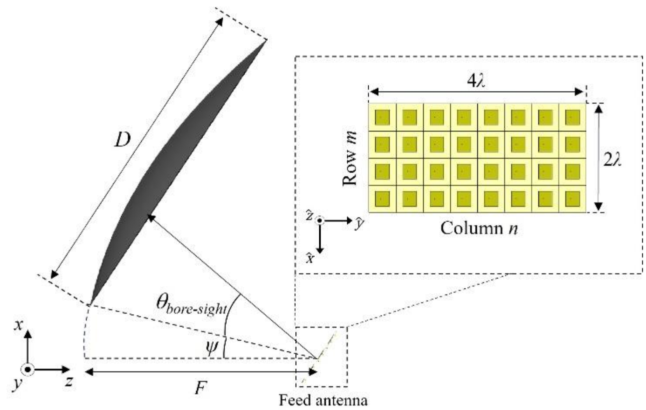

FIGURE 5. Geometry of the offset reflector antenna in the simulation setup.

TABLE 1. Offset reflector geometric parameters.

Parameters	Diameter	Focal point	Offset angle ψ	Reflector surface material	$\theta_{\text{bore-sight}}$
Values	10 m	6 m	0°	PEC	38°

Since it is difficult to realize the optimal mask $G(\theta, \phi)$ in Figure 2(b) using a practical antenna pattern, the beam synthesis method is applied to generate a pattern that approximates the optimal mask. The resulting synthesized pattern is shown in Figure 6. Using the proposed method, the synthesized pattern with a taper order of $N = 0.5$ is shown in Figure 6(a). The input weights used to generate the proposed pattern are calculated using equation (17), and the corresponding complex values are presented in Table 2. The complex vector applied to the antenna element located at (m, n) is presented in terms of the normalized amplitude (V/m) and phase (degree). Then the synthesized pattern of the PAF is obtained using the full-wave simulation with the Time Domain Solver in CST Studio Suite [32]. The realized gains at the upper and lower edges are 4.9 dBi and 1.4 dBi,

This article has been accepted for publication in IEEE Open Journal of Antennas and Propagation. This is the author's version which has not been fully edited and content may change prior to final publication. Citation information: DOI 10.1109/OJAP.2026.3696230

respectively, showing a difference of approximately 3.5 dB. This shows good agreement with the 4 dB gain difference between the upper and lower edges of the gain mask. Additionally, the synthesized pattern of the PAF using the cosecant-squared mask and the conventional horn antenna's pattern are shown in Figures 6(b) and 6(c), respectively. The pattern in Figure 6(b) is synthesized using a flat-top mask along the *x*-axis (*u*-cut) and a cosecant-squared mask along the *y*-axis (*v*-cut), with the same quadratic taper function applied to both masks. The synthesized pattern derived from the cosecant-squared mask has a rectangular shape that does not match the circular aperture area, thus increasing spillover loss. The horn consists of a rectangular waveguide section and a flared aperture section. The rectangular waveguide section has a cross-sectional size of 58 mm × 35 mm, while the flared aperture has an aperture size of 125 mm × 120 mm. The height of the waveguide section is designed to be 50 mm, and the height of the flare is designed to be 100 mm. The waveguide horn exhibits a bore-sight gain of 12.1 dBi. The gain at the reflector edge is 1.1 dBi in the horizontal (*u*-plane) and 5.3 dBi in the vertical plane (*v*-plane), corresponding to edge taper levels of 11.0 dB and 6.8 dB, respectively [33]. Consequently, the horn cannot provide uniform illumination for the offset reflector, which has an asymmetric structure. These three feed antenna patterns are presented with the gain mask in the *zx*-plane (asymmetric plane) in Figure 6(d). Radiation patterns (in *zx*-plane and *zy*-plane) obtained when illuminating the offset reflector with these three different feed patterns are shown in Figure 6(e) and Figure 6(f), respectively. The synthesized far-field patterns of the PAF are extracted and used as the feed source in CST's Integral Solver to obtain the far-field patterns of the reflector fed by PAF. When the reflector is illuminated using the proposed feed pattern, the bore-sight gain shows 48.2 dBi (corresponding to an aperture efficiency of 77.1%), while the SLL is –39.0 dB. These results demonstrate that the proposed method provides superior main lobe gain and sidelobe suppression performance compared with the results of the cosecant-squared mask (gain: 47.5 dBi, aperture Effi.: 65.6%, SLL: –35.8 dB) and a conventional horn antenna (gain: 47.8 dBi, aperture Effi.: 70.0%, SLL: –34.0 dB). Herein, the aperture efficiencies are calculated using the projected aperture of the reflector in the bore-sight direction [34]. Additionally, we evaluate the performance variation for different offset angle (ψ) cases using the proposed method. For an ψ of 10°, the reflector achieves a bore-sight gain of 47.8 dBi (aperture Effi. 74.6%), with an SLL of –39.9 dB. When the ψ is increased to 20°, a bore-sight gain is 47.7 dBi (aperture Effi. 75.3%), with an SLL of –44.7 dB. These results show that the proposed method maintains an aperture efficiency above 70% for all ψ cases while effectively suppressing the sidelobe level. The resulting aperture efficiency with the proposed method shows a degradation of approximately 3% compared to that obtained when the reflector is illuminated by the synthesized pattern based on the isotropic element patterns shown in Figure 4.

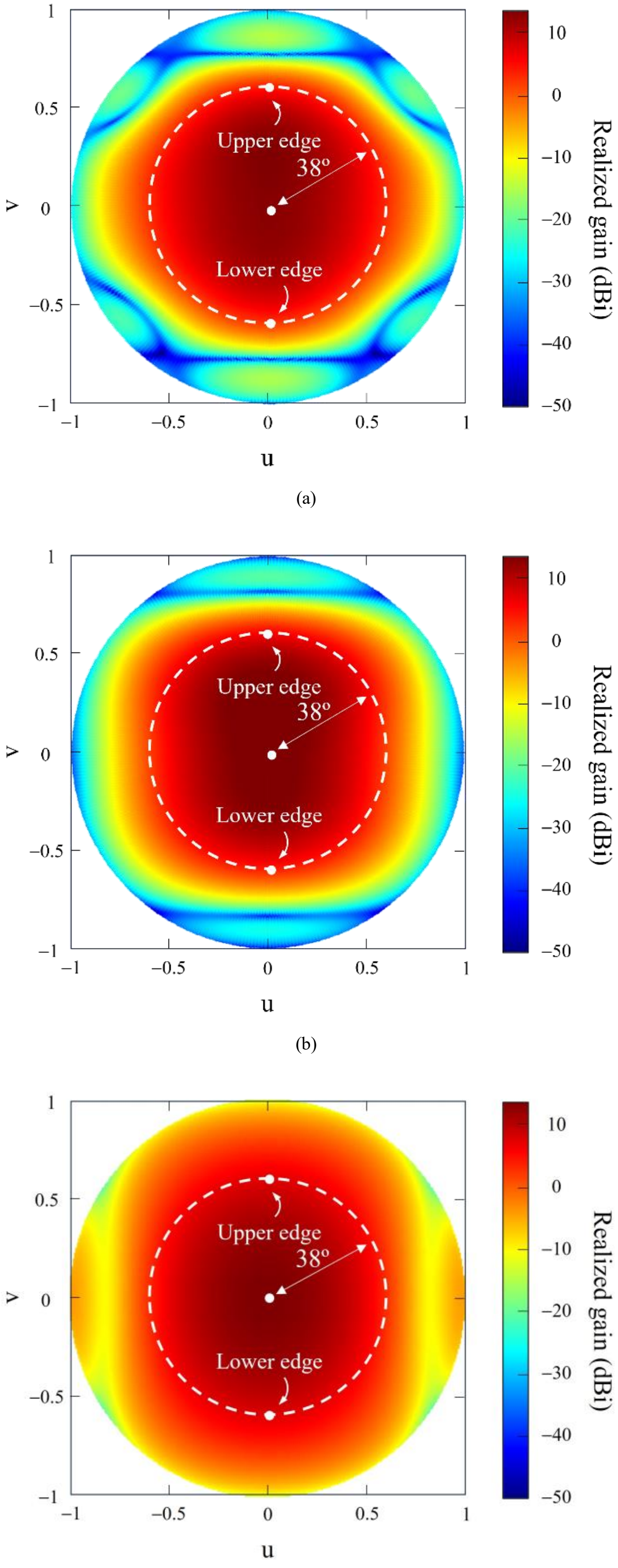

(a)
(b)
(c)

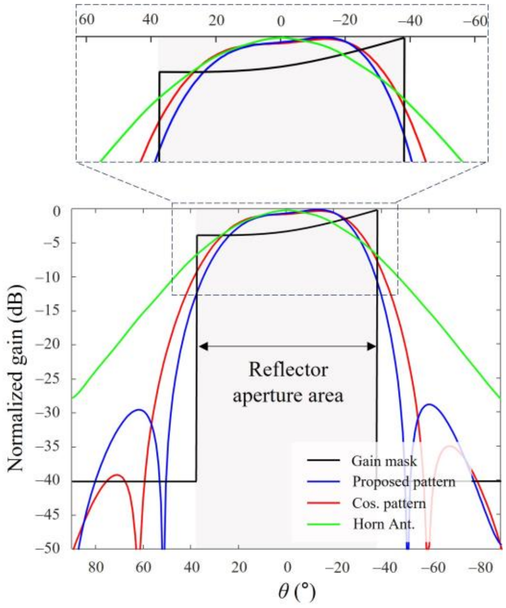

(d)

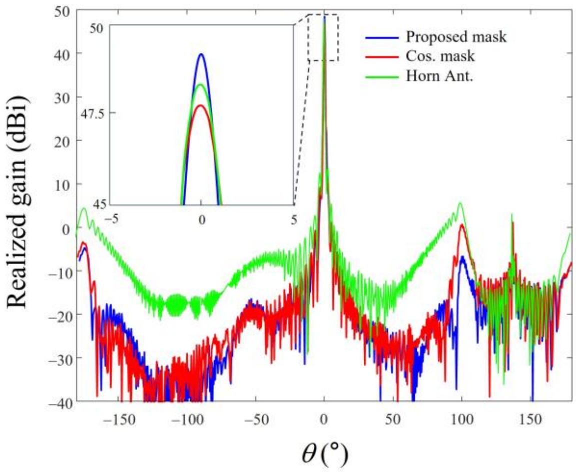

(e)

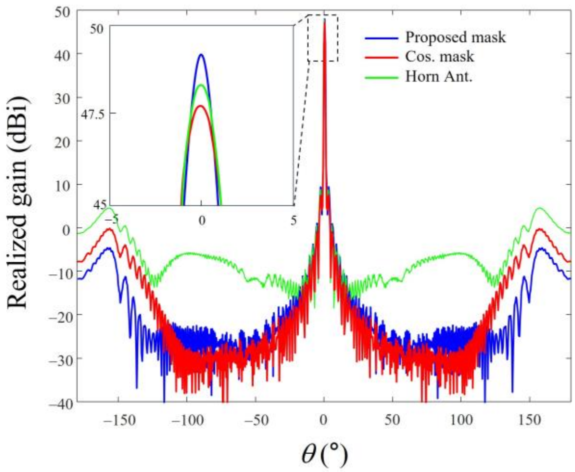

(f)

FIGURE 6. Feed antenna patterns and reflector patterns. (a) *uv*-plot of the proposed PAF pattern with *N* = 0.5. (b) *uv*-plot of the cosecant-squared mask based synthesized pattern. (c) *uv*-plot of the conventional horn antenna. (d) Radiation patterns of the feed antennas in the *zx*-plane. (e) PAFR radiation patterns in *zx*-plane. (f) PAFR radiation patterns in *zy*-plane.

TABLE 2. Complex signals of the 4 × 8 PAF antenna.

	Amplitude (V/m) ∠ Phase (degree)							
m	0.02∠ −140°	0.1∠− 180°	0.03∠ 65°	0.28∠ 4°	0.28∠ −4°	0.03∠ −65°	0.1∠1 80°	0.02∠ 140°
	0.06∠ −163°	0.1∠1 70°	0.33∠ 13°	1.00∠ 3°	1.00∠ −3°	0.33∠ −13°	0.1∠− 170°	0.06∠ 163°
	0.06∠ −163°	0.1∠1 70°	0.33∠ 13°	1.00∠ 3°	1.00∠ −3°	0.33∠ −13°	0.1∠− 170°	0.06∠ 163°
	0.02∠ −140°	0.1∠− 180°	0.03∠ 65°	0.28∠ 4°	0.28∠ −4°	0.03∠ −65°	0.1∠1 80°	0.02∠ 140°
	n							

Figure 7 shows the performance of the PAFR when the quadratic edge tapering is applied to the proposed mask. We sweep the quadratic edge taper order (N) and compare the radiation patterns of the PAFR in the *zx*-plane and *zy*-plane, as shown in Figure 7(a) and Figure 7(b), respectively. As the N increases, the aperture efficiency decreases while the SLL increases, showing a trade-off between the two characteristics. Figure 7(c) summarizes the results of the PAFR aperture efficiencies and the SLLs obtained by the proposed method and cosecant-squared mask method for different values of N. At $N = 0$ (without edge tapering), the aperture efficiencies of the reflector obtained by the proposed and the cosecant-squared-based methods are 78.9% and 65.6% respectively, with SLLs of −35.2 dB and −32.0 dB. At $N = 1.0$ (with strong edge tapering), the reflector's aperture efficiencies are 74.9% and 62.6% respectively, and the SLLs are −42.2 dB and −40.0 dB, respectively. Furthermore, for all values of N from 0 to 1, the reflector radiation pattern obtained with the proposed method exhibits higher aperture efficiency and SLL compared with the cosecant-squared method.

Table 3 summarizes the comparison between the proposed gain mask-based method and the CFM-based method, which is considered a state-of-the-art approach for gain maximization in PAFR [17], [18]. The CFM-based method achieves a bore-sight gain of 48.4 dBi (aperture Effi. 81.5%), with an SLL of −31.3 dB. However, since the basic CFM does not control the sidelobe level, an additional constrained optimization algorithm is required for SLL suppression. Moreover, the CFM-based method requires port-by-port full-wave EM simulations to determine the excitation weights of the PAF. Our proposed method achieves a bore-sight gain of 48.2 dBi (aperture Effi. 77.1%) and SLL of −39.0 dB, improving the SLL by approximately 7.7 dB compared with the CFM-based method. Furthermore, the sidelobe suppression can be controlled through the taper order N. As the proposed gain mask and excitation weights are derived directly from the geometry of reflector, full-wave simulations are not required for weight derivation. These results show that the proposed method is computationally efficient while maintaining high aperture efficiency and enhanced SLL suppression performance.

TABLE 3. Comparison between the proposed gain mask-based method and CFM.

Method	Gain (Aperture Effi.)	SLL	SLL controllability	EM simulation required
CFM	48.4 dBi (81.5%)	–31.3 dB	Limited; constrained optimization required	Yes
Proposed method	48.2 dBi (77.1%)	–39.0 dB	Controlled through taper order *N*	No

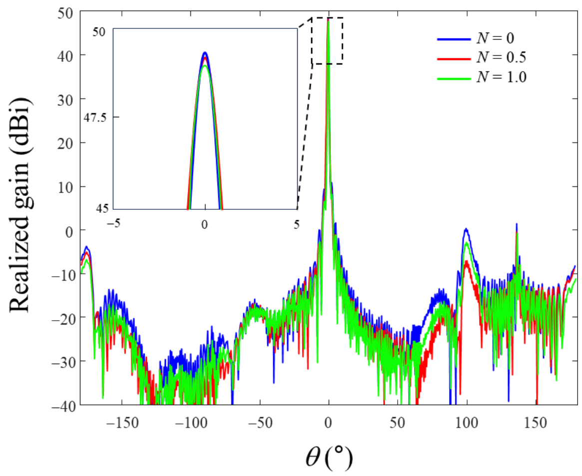

(a)

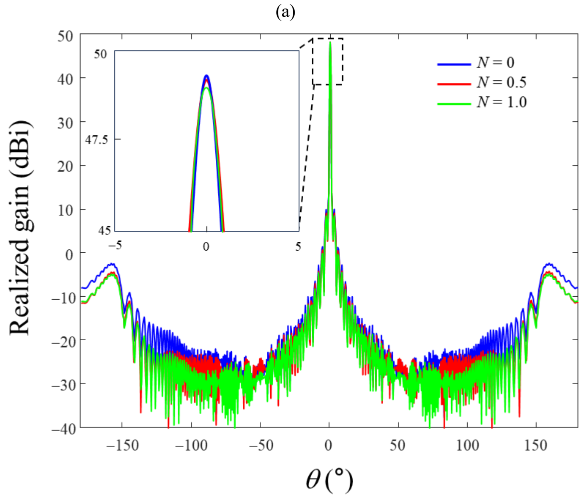

(b)

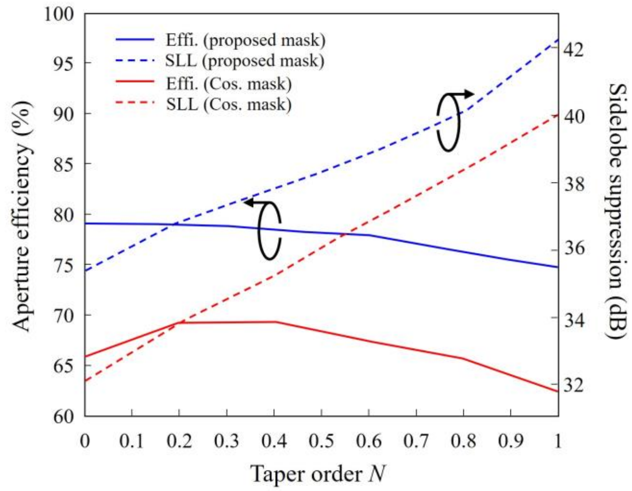

(c)

FIGURE 7. Aperture efficiencies and SLLs with differential tapering orders. (a) PAFR far-field pattern in *zx*-plane for *N* = 0, *N* = 0.5, and *N* = 1.0, based on the proposed method. (b) PAFR far-field pattern in *zy*-plane. (c) Comparison of PAFR aperture efficiencies and SLLs with the proposed method and the cosecant-squared mask method.

V. CONCLUSION

In this paper, we proposed a method to derive the optimal gain mask to enhance the aperture efficiency of a PAFR antenna. The optimal gain mask was obtained to uniformly illuminate the offset reflector's surface. The optimal gain mask was derived based on the square of the distances from the feed antenna to each point on the offset reflector surface. To generate a feed pattern similar to the optimal gain mask, a 4 × 8 array antenna was used as the feed antenna. Using this array antenna, beam synthesis was applied through the superposition of array patterns sampled at 1° intervals in both θ and ϕ. In addition, to achieve sidelobe suppression, quadratic taper function was applied to the derived optimal gain mask. We then illuminated the reflector using three feed patterns: a synthesized beam based on the proposed mask, a synthesized beam following a cosecant-squared mask, and a single horn antenna pattern. In this case, the same quadratic tapering order of N = 0.5 was applied to both the proposed mask and the cosecant-squared mask. The gain mask-based method showed a bore-sight gain of 48.2 dBi and an SLL of –39.0 dB, representing improvements compared with the results obtained using the cosecant-squared-based pattern (47.5 dBi and –35.8 dB) and the horn antenna pattern (47.8 dBi and –34.0 dB). These results demonstrated that the proposed gain mask and beam synthesis method are effective in achieving high aperture efficiency and sidelobe suppression performance.

REFERENCES

[1] S. Huber, M. Younis, G. Krieger, A. Moreia, and W. Wiesbeck, "A Reflector Antenna Concept Robust Against Feed Failures for Satellite Communications," *IEEE Trans. Ant. Propag*., vol. 63, no. 4, pp. 1218-1224, Dec. 2014.

[2] R. Roy, R. Kumar, and V. K. Singh, "A Wideband Dual Polarised Hat Feed-Based Ku-Based Ku-Band Reflector Antenna for Man Portable Satcom Application," *Defense Science Journal*, vol. 74, no. 6, pp. 904-910, Nov. 2024.

[3] C. Im, W. Seo, S. Park, K. Kim, S. Park and H. Choo, "Design of a Deployable Broadband Mesh Reflector Antenna for a SIGINT Satellite System Considering Surface Shape Deformation," *MDPI Sensors*, vol. 24, no. 2, pp. 1-12, Jan. 2024.

[4] D. Stanescu, and A. Buzducea, "An Overview of Satellite Link Budget Sensitivity Based on Digital Modulation Schemes in Multi-Orbit Satellite Networks," *MDPI Appl. Sci*., vol. 15, no. 7, pp. 1-20, Mar. 2025.

[5] M. Darwish, and H. Hassani, "Wideband Transmitarray Antenna Based on Two-Layer Aperture-Coupled Metasurface Unit Cell," *J. Electromagn. Eng. Sci*., vol. 25, no. 5, pp.401-410, Sep. 2025.

[6] M. Balasubramanian, and D. H. Werner, "An Efficient Curvature-Based Synthesis Methodology for Rotationally Symmetric Shaped Reflector Antennas," *IEEE Open J. Antennas. Propag*., vol. 6, no. 1, pp. 181-192, Feb. 2025.

[7] S. Shrestha, and D. Choi, "Rain Attenuation Over Terrestrial Microwave Links in South Korea," *IET Microw. Antennas Propag*., vol. 11, no. 7, pp. 1031-1039, Jun. 2017.

[8] S. Zhang, J. Du, and P. Li, "Design of Shaped Offset Cable Mesh Reflector Antennas Considering Structural Flexible Property," *IET Microw. Antennas Propag*., vol. 11, no. 7, pp. 1024-1030, May. 2017.

[9] Y. Huang, W. Yu, Q. Lin, W. Li, and Y. Feng, "The Development of a Spaceborne SAR Based on a Reflector Antenna," *MDPI Remote Sens.*, vol. 17, no. 14, pp. 1-29, Jul. 2025.

[10] A. Meguro, K. Shintate, M. Usui, and A. Tsujihata, "In-orbit Deployment Characteristics of Large Deployable Antenna Reflector Onboard Engineering Test Satellite VIII," Acta Astronaut., vol. 65, pp. 1306-1316, May. 2009.

[11] J. Huang, H. Wang, D. Han, C. Lee, S. Jo, C. Seo, S. Kim, S. Yoon, J. Yoon, and S. Park, "A Force-Based Elastic Mesh Model for Electrical Property Analysis of Reflector Antennas," *J. Electromagn. Eng. Sci*., vol. 25, no. 6, pp. 619-626, Nov. 2025.

[12] M. Biguesh, S. Valaee, B. Champagne, M. H. Bastani, and F. Farzaneh, "A Robust Sidelobe Canceller for Reflector Antenna Using Signal Subspace Eigenvectors," *Revue HF*, 2001.

[13] D. A. Pujara, S. Sharma and S. B. Chakrabarty, "Improving the Beam Efficiency of an Offset Parabolic Reflector Antenna for Spaceborne Radiometric Applications," *Prog. Electromagn. Research C*, vol. 10, pp. 143-150, Sep. 2009.

[14] J. Park, C. Im, and H. Choo, "Design of Koch-Curved LPDA Antenna With Optimized Beamwidth to Improve the Aperture Efficiency of Reflector Antennas," *IEEE Access*, vol. 13, pp. 106747-106758, Jun. 2025.

[15] J. R. Fisher, "Phased Array Feeds for Low Noise Reflector," *NRAO Electronics division internal report*, pp. 101-123, Sep. 1996.

[16] M. Cooley, "Phased Array Fed Reflector (PAFR) Antenna Architectures for Space-Based Sensors," *IEEE Aerospace Conference*, pp. 1-11, Mar. 2015.

[17] A. Salmi, A. Lehtovuori and V. Viikari, "On Realized Gain-Optimal Feeding Coefficients of Antenna Arrays," *IEEE European Conf. on Antennas and Propagation (EuCAP)*, Florence, Italy, pp. 1-5, Mar. 2023.

[18] B. Saka and E. Yazgan, "Pattern Optimization of a Reflector Antenna with Planar-Array Feeds and Cluster Feeds," *IEEE Trans. Ant. Propag.,* vol. 45, no. 1, pp. 93-97, Jan. 1997.

[19] R. J. Acosta, "Active Feed Array Compensation for Reflector Antenna Surface Distortions," *NASA Technical Memorandum 100826*, Jun. 1988.

[20] N. Michishita, J. Shinohara, Y. Yamada, M. T. Islam, and N. Misran, "Design of an Array Feed Offset Parabolic Reflector Antenna by Using Electromagnetic Simulations and Measured Results," *ACES Journal*, vol. 28, no. 12, pp. 1250-1256, Dec. 2013.

[21] J. Yang, "Calculation of Aperture Efficiency of Reflector Antenna with the Measured Far-field Function of Its Feed in Ludwig's Third Definition," *IEEE European Conf. on Antennas and Propagation (EuCAP)*, Dusseldorf, Germany, pp. 1-4, Mar. 2021.

[22] B. Xiang, C. Wang, and P. Lian, "Effect of Surface Error Distribution and Aberration on Electromagnetic Performance of a Reflector Antenna," *International Journal of Antennas and Propagations*, vol. 2019, pp. 1-15, May 2019.

[23] V. Manohar and Y. Rahmat-Samii, "Understanding the Radiation Characteristics of Metal-Only, Low-Profile, Offset Stepped Parabolic Reflector Antennas: Simulation, Analysis, and Measurement," *IEEE Trans. Ant. Propag*., vol. 69, no. 8, pp. 5078-5083, Aug. 2021.

[24] C. A. Balanis, *Antenna Theory*: *Analysis and Design*, 4th ed., Hoboken, NJ, USA: Wiley, 2016, ch. 7, pp. 875-923.

[25] W. L. Stutzman and G. A. Thiele, *Antenna Theory and Design*, 3rd ed., John Wiley & Sons, 2012.

[26] M. J. Pagones, "Gain Factor of an Offset-Fed Paraboloidal Reflector," *IEEE Trans. Ant. Propag*., vol. 16, no. 5, pp. 536-541, Sep. 1968.

[27] J. F. Kauffman, W. F. Croswell, and L. J. Jowers, "Analysis of the Radiation Patterns on Reflector Antennas," *IEEE Trans. Ant. Propag*., vol. 24, no. 1, pp. 53-65, Jan. 1976.

[28] Y. Zhang, H. Liu, and X. Liu, "Influence of the Reflector Subtended Angle on the Performance of Parabolic Antennas with Feed Displacement," *MDPI Electronics*, vol 11. No. 17, pp. 1-10, Aug. 2022.

[29] C. Im, S. Youn, T. Lim, and H. Choo, "Design of a Compact Log Periodic Dipole Array Antenna for Broadband and High-Power Beam Synthesis Using Superposition," *J. Electromagn. Eng. Sci*., vol. 24, no. 3, pp. 234-242, Sep. 2023.

[30] S. Prasad, M. Meenakshi, and P. H. Rao, "Three-Dimensional Shaped and Contour Pattern Synthesis with Multiple Beam Approach," *Microw. Opt. Tech. Letters*, vol. 65, pp. 873-880, Dec. 2022.

[31] J. R. Mohammed, A. J. Abdulqader, and R. H. Thaher, "Antenna Pattern Optimization via Clustered Arrays," *Prog. Electromagn. Res. M*, vol. 95, pp. 177-187, Aug. 2020.

[32] *CST Studio Suite: Electromagnetic Field Simulation Software*. Accessed: Apr. 6, 2026. [Online]. Available: http://www.cst.com

[33] H. Wei and Z. Li, "Analysis of the Reflector Antenna's Feed Taper Level," Proc. *IEEE Int. Conf. Computer and Communication Engineering Tech.* (*CCET*), pp. 213-217, Aug. 2019.

[34] ITU-R *Recommendation S.672, Satellite antenna radiation pattern for use as a design objective*, 1997.

MINSANG YOON received the B.S. degree in electronic and electrical engineering from Hongik University, Seoul, South Korea, in 2025, where he is currently pursuing the M.S. degree in electronic and electrical engineering. His research interests include array antennas, signal processing, machine learning, and satellite communications.

CHANGHYEON IM received the B.S. degree in electronic and electrical engineering from Hongik University, Seoul, South Korea, in 2021, where he is currently pursuing Ph.D. degree in electronic and electrical engineering. His research interests include mesh reflector antenna, 5G application, wireless power transfer, and ultra-wideband antenna.

CHANGSEONG KIM received the B.S. and integrated M.S./Ph. D. degree from the Department of Electrical and Computer Engineering, Ajou University, Suwon, South Korea, in 2015, 2021, respectively. Since 2021, He has been a researcher with Hanwha Systems. Pangyo, South Korea, His research interests include the tropospheric wave propagation, array antenna, reflector antenna.

WONGU SEO received the B.S. degrees and M.S. degrees in electrical engineering from Chungnam National University, in 2014 and 2016 respectively. Since January 2016, he is currently working in the tactical communication system team of Hanwha Systems. His major research fields include Satellite Antennas, Electronic Warfare Systems, and Tactical Communication Systems.

SEULGI PARK received the B.S. degrees and M.S. degrees in electrical engineering from Hongik University, in 2006 and 2008 respectively. He worked at Electronic Warfare Research Center of LIG Nex1 corporation from 2008 to 2013, and from 2013 to 2016 at DMC Research Center of Samsung Electronics Corporation. Since January 2017, he is currently working in the tactical communication system team of Hanwha Systems. His major research fields include electronic warfare transmission/reception antennas, electronic warfare systems, and tactical communication systems.

HOSUNG CHOO received his B.S. degree in radio science and engineering from Hanyang University, Seoul, Republic of Korea, in 1998, and his M.S. and Ph.D. degrees in electrical and computer engineering from the University of Texas at Austin in 2000 and 2003, respectively. In September 2003, he joined the School of Electronic and Electrical Engineering, Hongik University, Seoul, Korea, where he is currently a full-time professor. His principal areas of research are the use of the optimization algorithm in developing antennas and microwave absorbers. His studies include the design of small antennas for wireless communications, reader and tag antennas for RFID, and on-glass and conformal antennas for vehicles and aircraft.